



Since January 2020 Elsevier has created a COVID-19 resource centre with free information in English and Mandarin on the novel coronavirus COVID-19. The COVID-19 resource centre is hosted on Elsevier Connect, the company's public news and information website.

Elsevier hereby grants permission to make all its COVID-19-related research that is available on the COVID-19 resource centre - including this research content - immediately available in PubMed Central and other publicly funded repositories, such as the WHO COVID database with rights for unrestricted research re-use and analyses in any form or by any means with acknowledgement of the original source. These permissions are granted for free by Elsevier for as long as the COVID-19 resource centre remains active.



# Facile fabrication of reinforced sub-micron fibrous media with hierarchical structure compounded thermally for effective air purification in application

Mengjuan Zhou<sup>a</sup>, Lulu Shi<sup>a</sup>, Hongyu Dai<sup>a</sup>, Akampumuza Obed<sup>b</sup>, Penghong Liu<sup>a</sup>, Jiajun Wu<sup>a</sup>, Xiaohong Qin<sup>a,\*</sup>, Rongwu Wang<sup>a,\*</sup>

<sup>a</sup> Key Laboratory of Textile Science and Technology of Ministry of Education, College of Textiles, Donghua University, Shanghai 201620, China

<sup>b</sup> Uganda Industrial Research Institute, Nakawa Industrial Area, P.O. Box 7086, Kampala, Uganda

## ARTICLE INFO

### Keywords:

Free surface electrospinning  
Sub-micron fibers  
Hierarchical structure  
Thermal bonding process  
Air filtration

## ABSTRACT

Air pollution has steadily worsened in recent years, and the coronavirus disease 2019 has been spreading since 2020. The electrospun fibrous filters present superior filtration performance, while the low mechanical property and yield of them limit their applications, which must be addressed urgently. Herein, polyacrylonitrile (PAN) sub-micron fibrous membrane with hierarchical structure was easily manufactured using free surface electrospinning in mass production for air purification. The “sandwich” structured fibrous filter was thermally bonded with bi-component nonwoven through traditional bonding procedures, due to melting and bonding of the cortex of bi-component fibers, in which the electrospun fibrous web as the mid layer with tortuous channels showed superior filtration performance for aerosol particles with diameter of 260 nm, which could effectively intercept different-sized particles suspended in the air. In addition, the impact of the processing parameters on the characteristics and filtration mechanisms of thermally bonded composite materials was thoroughly investigated. The results showed that composite material with “dendrites” and “axon” morphologies presented the best formability, outstanding peeling strength and breaking strength, and steady filtration performance, following an easy through-air bonding procedure, making it useful for post-processing in air purification. The reinforced composite filter, which is thermally bonded with sub-micron fibers with high yield and nonwoven, is save-energy and has a low operation cost, indicating its promising commercial possibilities.

## 1. Introduction

Air pollution is one of the most significant sources of environmental pollution, and it has grown in prominence as a result of industrialization, attracting increased societal attention in recent years [1]. Taking an example of suspended fine particulate matters (PMs) with an aerodynamic diameter of less than 2.5  $\mu\text{m}$  (PM<sub>2.5</sub>), these can easily penetrate the human lungs, increasing the incidence of respiratory and heart diseases [2,3]. In addition, there is an increasing risk posed by the emergence of respiratory infections, for instance, the sudden emergency and rapid spread of the coronavirus disease 2019 (COVID-19), whose primary dissemination route is droplet transmission [4–6]. As a result, the professional anti-haze masks are required to reduce or eliminate the risk posed to the human body by air pollutants (aerosols and viruses). Furthermore, the performance of precision instruments, as well as the atmosphere of enclosed public spaces such as hospitals and airports, are heavily reliant on the efficient air purification. Thus, the deployment of

air systems with superior filtration properties would ensure the safety of human and the unintended performance of such equipment [7,8].

Electrospinning process produces a disordered accumulation of sub-micron or micron fibers, resulting in a highly porous membrane with distinct properties [9,10]. This is characterized by a uniform packing density and tunable network geometry, both of which are conducive to filtering fine particles [11–13]. The arrangement and multi-level structure of fibrous membrane with different fiber diameters show a positive effect on the filtration performance of fibrous filters [14,15]. While, only scanty work is available on the fabrication of sub-micron fibrous webs with hierarchical structure as an air filter. In practice, electrospun sub-micron fibrous materials with low strength need to be combined with non-woven fabric to meet mechanical strength requirements. However, due to the low interfacial force and bonding strength between the sub-micron fibrous membranes and the substrate layer, they may easily peel off or fray during post-processing (composite processing and filter preparation) and in the actual applications. However, if the two layers

\* Corresponding authors at: College of Textiles, Donghua University, Shanghai 201620, China.

E-mail addresses: [xhqin@dhu.edu.cn](mailto:xhqin@dhu.edu.cn) (X. Qin), [rw@dh.u.edu.cn](mailto:rw@dh.u.edu.cn) (R. Wang).

<https://doi.org/10.1016/j.seppur.2022.120726>

Received 23 November 2021; Received in revised form 18 February 2022; Accepted 20 February 2022

Available online 24 February 2022

1383-5866/© 2022 Elsevier B.V. All rights reserved.

were superimposed directly, the product's safety would be jeopardized. The main effective ways to improve the adhesion force between them are chemical and thermal bonding processes. The thermal bonding process takes advantage of the thermoplastic properties of polymers, in which the polymer softens, diffuses, flows, adheres between the fibers, and finally solidifies after cooling down to form a bonding point. This method is widely used in the preparation and processing of non-woven materials because the finished products, which do not contain chemical adhesives, are environmental-friendly and effective.

The thermal bonding process is mainly classified into three categories, extra-sonic composite method [16], through-air method [17], and hot-rolled bonding method [18]. Among of them, the through-air and hot-rolled bonding processes are used commercially. In the through-air bonding process, the nonwoven fabrics with thermoplastic properties are heated with hot air to reach the melting point, melted to produce viscous flow, and then condense at the fiber intersections. As for the bonding process, fibrous materials are heated and pressurized by one or two pairs of heated steel rollers, causing some fibers to melt, flow, diffuse, bond, cool down, and be strengthened, which does not require a binder preparation station and is energy-efficient, low-cost, and widely used in actual production [18,19]. Previous research on electrospun fibrous materials as air filters focuses primarily on the front-end electrospinning preparation and materials' properties, ignoring the subsequent composite process, which is critical in practical applications. Nguyen and Kim [20] chose a commercial heat roller to manufacture PAN nanofiber air filter laminated with non-woven fabrics using heat and pressure, which showed the material with a sandwich structure (non-woven fabric/PAN nanofiber/non-woven fabric) possessed a high filtration efficiency with structural stability, while the work mainly focused on optimizing the electrospinning conditions. Till now, there is a rare detailed report about the influence of the bonding composite process on the properties and air-filtration performance of the electrospun

fibrous filter.

In this study, a PAN sub-micron fibrous membrane with hierarchical structure was simply prepared via free surface electrospinning for large-scale production as an air filter cartridge (Fig. 1(a)), in which the upper and lower substrates were the polyethylene/polypropylene (PE/PP) bi-component composite hot-air nonwoven fabric, preparing a "sandwich"-structure compound fibrous filter (nonwoven fabric/sub-micron fibers/nonwoven fabric). First, the effect of fiber diameter, areal density, and fibrous web structure on the filtration performance of PAN fibrous membrane was investigated. Then, the composite materials resembling a sandwich structure were compounded via two different thermally bonding processes (i.e., hot-rolled and through-air bonding processes) (Fig. 1(b, c)), respectively, to improve interlaminar fracture toughness and suppress the delamination in laminated non-woven fibers. Furthermore, the impact of process parameters (calender temperature and feeding speed, as well as nip pressure in hot-rolled process; heating temperature and time in through-air bonding process) on the properties of composite materials was investigated in order to ensure excellent filtration performance and mechanical properties for post-processing in air purification, which was conducive to practical applications.

## 2. Experimental

### 2.1. Materials

Polyacrylonitrile (PAN,  $M_w = 85,000$ ) with a material density of  $1.184 \text{ g cm}^{-3}$  was purchased from Shanghai Chemical Fibers Institute. N-dimethylformamide (DMF, AR) was supplied by Sinopharm Chemical Reagent Co., Ltd., China. Hot-air non-woven fabric of sheath-core polyethylene/polypropylene (PE/PP) bi-component composite fibers (the areal density is  $25 \text{ g m}^{-2}$ , the sheath/core ratio is 1: 1, and the fiber

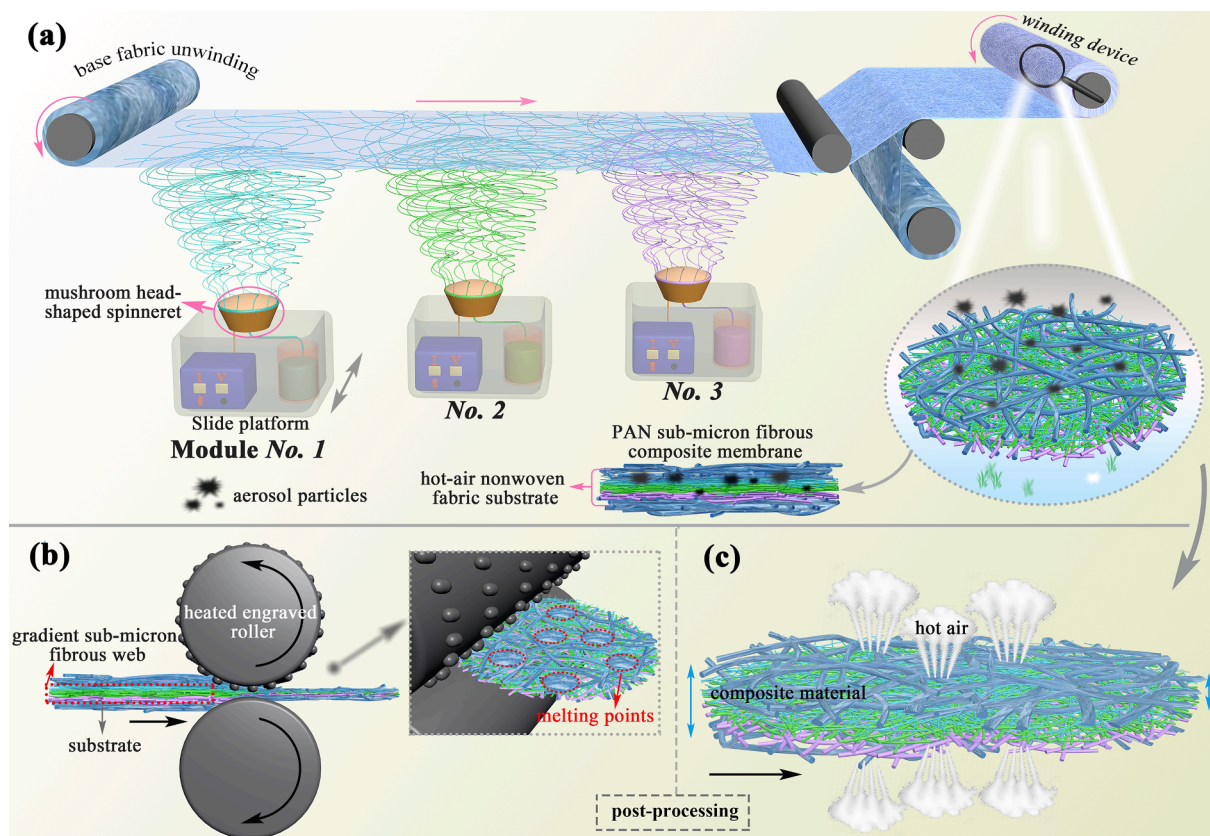


**Fig. 1.** Schematic diagrams of (a) free surface electrospinning with mushroom head-shaped spinnerets for preparing fibrous membranes with hierarchical structure, (b) the hot-rolled bonding process with point bonding, and (c) through-air composite processes for the composite materials.

diameter is 18  $\mu\text{m}$ ) possesses the negligible filtration efficiency (5%) and pressure drop (4 Pa) at airflow velocity of 5.3  $\text{cm s}^{-1}$  for collecting the electrospun sub-micron fibers, provided by Sanming Kangerjia sanitary products Co., Ltd., Fujian. All reagents were used without further purification.

## 2.2. Preparation of electrospun PAN sub-micron fibrous membranes

PAN powder was dried in an oven for 3 h, then it was dissolved in DMF and stirred magnetically at room temperature for 24 h to prepare precursor solutions with mass concentrations of 10 wt%, 12 wt%, and 14 wt%, respectively.

A compensating phase modular continuous electrospinning line, consisting of a base fabric unwinder, a drying device, a tension control device and a fabric winding device has been developed by our group [21]. Its electrospinning main box contains multiple sets of modules with mushroom-head shaped spinnerets, a sliding platform, a solution reservoir, a peristaltic pump, and a high voltage direct-current power supply, as displayed in Fig. 1(a). Separate electrospinning modules could eliminate the problems of electric field interferences between jets and capillary blockage, resulting in a homogeneous sub-micron fibrous membrane with excellent filtration performance. Furthermore, the output speed of 0–1  $\text{m min}^{-1}$  and width of 1–1.6 m is 150 times that of traditional single-needle electrospinning; this is an important step toward industrializing sub-micron fiber production.

14 wt%, 12 wt%, and 10 wt% PAN solutions were separately placed at one of the modules, and the homogeneous sub-micron fibrous membranes with different areal densities (0.2, 0.5, 1.0, 1.5, and 2.0  $\text{g m}^{-2}$ ) were produced by regulating the feeding speed of the substrate fabric. The voltage for each module was 55 kV, and the supply rates for all solutions were the same at 80  $\text{ml h}^{-1}$ . The electrospun fibers were deposited on the surface of a traversing substrate 18 cm away from the spinneret. The slide platform moved back and forth at a speed of 9  $\text{m min}^{-1}$ , maintaining the uniformity of the prepared fibrous webs. Following deposition, the membrane was transferred to the drying device to vaporize the residual solvent.

The electrospun fibrous membranes with hierarchical structure were abbreviated as PAN-x/y/z. Accordingly, three types were fabricated: (a) PAN-10/12/12, in which 12 wt% PAN solutions were placed in No. 1 and No. 2 modules, and 10 wt% solution was added in No. 3 module; (b) PAN-10/14/14, in which 14 wt% PAN solution was put in No. 1 and No. 2 modules, and 10 wt% solution was placed in No. 3 module; (c) PAN-10/12/14, in which 14 wt%, 12 wt%, and 10 wt% PAN solutions were separately placed in No. 1, No. 2, and No. 3 modules. Each layer's areal density was controlled within  $0.5 \pm 0.1 \text{ g m}^{-2}$ , and the overall areal density of obtained composite membranes was kept within  $1.5 \text{ g m}^{-2}$ . In addition, the relative humidity and temperature of the electrospinning main box were kept at  $35 \pm 5 \text{ \%RH}$  and  $25 \pm 3 \text{ }^\circ\text{C}$ , respectively.

## 2.3. Preparation of thermally bonded composites by a hot-rolled bonding process

The hierarchical-structured PAN-10/12/14 sub-micron fiber membrane was placed between two layers of PE/PP hot-air nonwoven fabrics chosen as the substrate layer (detail explanation seen in Supplementary information), forming a "sandwich" structure. The composite material was next subjected to a hot-rolled bonding process that included point and surface bonding (PB and SB) operations, as shown schematically in Fig. 1(b) and Fig. S1 (Supplementary information). In line with the melting point of bi-component PE/PP fibers and PAN sub-micron fibers (Fig. S2), the hot-rolled temperatures of 100  $^\circ\text{C}$ , 110  $^\circ\text{C}$ , and 120  $^\circ\text{C}$  were chosen, and the process was carried out at a rolling speed of 1  $\text{m min}^{-1}$  and a hot-rolling pressure of 3 MPa.

The linear speed, temperature, and pressure of the roller in the bonding process were the detailed parameters affecting the performance of composite materials, which were analyzed via orthogonal experiment

and then all the factors were selected to design a whole factor test scheme (Table S1).

## 2.4. Preparation of thermally bonded composites by a through-air composite process

The obtained composite material was additionally subjected to the flat-net through-air penetration bonding procedure in order to create a through-air thermally bonded nonwoven, as shown in Fig. 1(c). In addition, the impact of process parameters (through-air temperature and processing duration) on the materials' properties was investigated, as shown in Table S2.

## 2.5. Characterization

The surface morphology of sub-micron fibrous membranes was characterized by a scanning electron microscopy (SEM, TM3000, Hitachi Group, Japan), and fiber diameters were calculated from SEM images using Nanomeasure 1.2 software. The samples' thickness and weight were determined using a thickness gauge (YG141N, Nantong Hongda Instruments Co., Ltd., China) and an electronic balance (MS105DU, Mettler-Toledo Group, Switzerland), respectively. The pore size distribution of fibrous webs was determined by a capillary flow porometer (POROLUXTM 100 FM, IB-FT Germany) with wetting fluid (surface tension of 16  $\text{mN m}^{-1}$ ). The peeling strength of the prepared composite materials was evaluated using a fiber strength elongation tester (LLY-06E, China), and the samples (5  $\times$  30 mm) were clamped at the crosshead with a gauge length of 20 mm and a crosshead speed of 10  $\text{mm min}^{-1}$  in the testing procedure, as shown in Fig. S3. Each group of samples was measured five times and the average was calculated. The mechanical properties of the composites were examined by an extensometer (YG028-500, China). The bending properties of the materials were tested by an electronic fabric stiffness instrument (LLY-01, China) at a test angle of 41.5 $^\circ$  and a propulsion speed of 4  $\text{mm s}^{-1}$ . Six samples were cut longitudinally and transversely, respectively, with a dimension of 250  $\times$  25 mm. The bending stiffness of the samples was calculated using the formula:  $G = m \times L^3 \times 10^{-3}$ , where  $G$  is the bending stiffness of the average unit width ( $\text{mN cm}$ ),  $m$  is the mass per unit area of the sample ( $\text{g m}^{-2}$ ), and  $L$  is the average bending length of the sample ( $\text{cm}$ ). The air permeability was tested through a fully automatic permeability instrument (YG461E, Ningbo Spinning Instrument, China) under pressure of 100 Pa, according to Standard GB\_T5453: 1997.

The filtration performance (filtration efficiency and pressure drop) of the samples was measured by an automated filtration testing machine (Model 8130, TSI Group, America). The machine operates by spraying electro-neutral solid monodisperse solid NaCl particles having a median diameter of 260 nm on an effective area of 100  $\text{cm}^2$ . The test was operated at room temperature with an air face velocity of 5.33  $\text{cm s}^{-1}$ , regarded as the industrial testing standard according to the latest USA standard: IEST-RP-CC52.2–2007 and European standard: EN779: 2012 for air filters. For accuracy of the results, five different parts of each sample were tested, and the results were expressed as the average of these values.

## 3. Results and discussion

### 3.1. Pristine PAN composite membranes with hierarchical structures

#### 3.1.1. Morphology

The pristine sub-micron fibrous monolayers had a smooth surface morphology with no beads, and fibers were uniformly distributed within the membrane, as shown in Fig. 2(a–c). Fiber diameters increased from 142 to 400 nm with the coefficient of variation (C.V.) ranging from 17.5% to 24.6%, which was attributed to the rising concentration of PAN precursor solutions (Fig. 2(d–f)). As the solution concentrations increased, the viscosity increased too, and the accompanying rise in

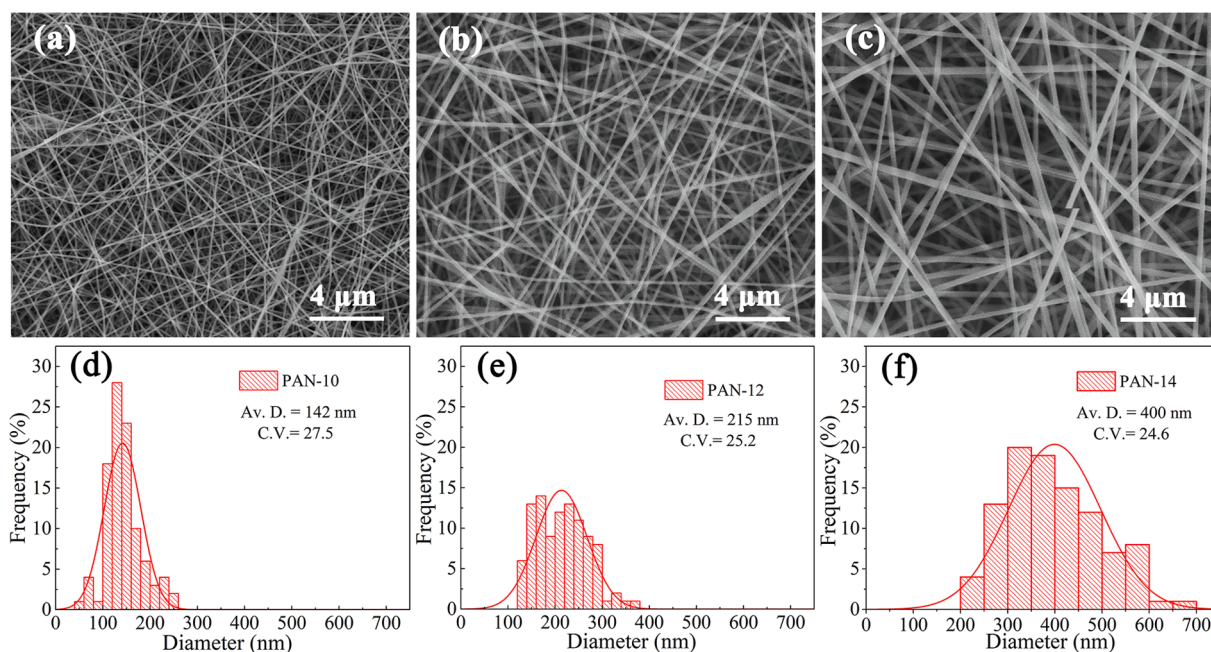


Fig. 2. (a–c) SEM images and (d–f) fiber diameter distributions of PAN-*x* sub-micron fibers ((a, d) PAN-10, (b, e) PAN-12, and (c, f) PAN-14).

intermolecular forces made it more difficult to draft the jets forming sub-micron fibers in the electrospinning process. Similarly, the pore size of fibrous membranes followed the same trend as fiber diameters (Fig. S4 (a)). This was impacted by the areal density and stacking pattern of fibrous webs, further affecting the material's filtration performance [22]. For fibrous membranes with the same areal density, the fiber number per unit area and packing density decreased with the increase of fiber diameter, resulting in a larger average pore size.

### 3.1.2. Structure

The structure of PAN sub-micron fiber membranes was designed in order to improve the filtration property. As shown in Fig. 3(a), the hierarchical-structured PAN fibrous webs were made up of triple layers

through varying two or three types of fiber diameters (PAN-10/14/14, PAN-10/12/12, and PAN-10/12/14), and the fibrous webs with the same fiber diameter for triple layers (homogeneous structure) were used as references. The hierarchical structure of PAN-10/14/14 sample was representative, as exhibited in Fig. S5, and some fine fibers overlapped on the top of the coarse fibrous layer, which reflected the difference in fiber diameters between the layers in the hierarchical-structured fibrous membrane. Fig. 3(b) shows the cross-sectional image of PAN-10/14/14 sample.

The pore size distribution and average pore sizes of the prepared PAN sub-micron fibrous membranes with various shapes but a comparable areal density of  $\sim 1.5 \text{ g m}^{-2}$  were displayed in Fig. 3(d, e). The average pore sizes of PAN-*x* ( $x = 14, 12,$  and  $10$ ) fibrous membranes with

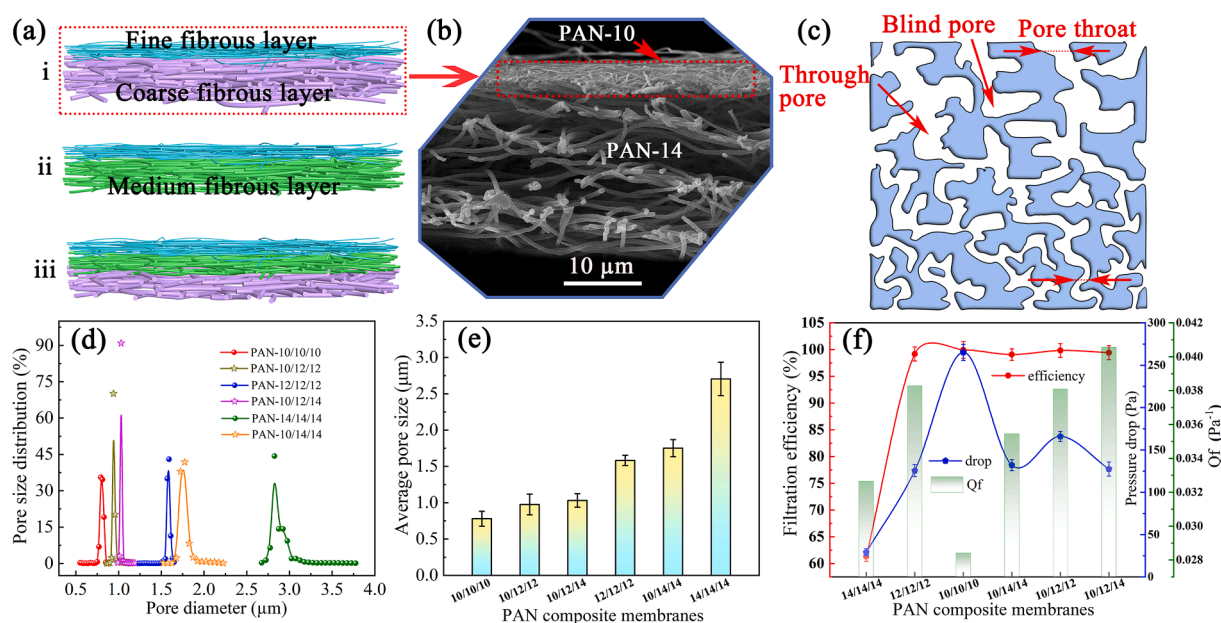


Fig. 3. (a) A schematic illustration of materials' structures, (b) the cross-sectional SEM image of PAN-10/14/14 fibrous membrane, (c) pore structure inside PAN-10/12/14 fibrous membrane; (d) the pore size distributions, (e) average pore sizes, and (f) filtration-performance parameters of PAN hierarchical sub-micron fibrous membranes with hierarchical structures.

homogenous structure were 2.705  $\mu\text{m}$ , 1.583  $\mu\text{m}$ , and 0.779  $\mu\text{m}$  (Fig. 3 (e)), respectively, and the pore size distributions steadily shrunk (Fig. 3 (d)). Nonetheless, when PAN-12/12 and -14/14 bilayers were combined with PAN-10 monolayer, their average pore sizes (PAN-10/12/12 and PAN-10/14/14) decelerated fast to 0.976  $\mu\text{m}$  and 1.752  $\mu\text{m}$ , separately, with a left-shift pore size distribution. PAN-10/12/14 with tri-layer structure, on the other hand, had an average pore size of 1.031  $\mu\text{m}$ , which was similar to that of PAN-10/12/12 sample. According to the findings, compounding with a PAN-10 fine fibrous layer with a smaller pore size had a substantial impact on the pore size of the composite material.

### 3.1.3. Filtration performance

The comparison with filtration performances was drawn in Fig. S4 (b–d) for pristine PAN fibrous monolayers with homogeneous internal structures and various areal densities. For PAN-10 and -12 samples with average fiber diameters of  $\sim 142$  nm and  $\sim 214$  nm, separately, the filtration efficiency of them improved dramatically as the areal density increased from 0.2  $\text{g m}^{-2}$  to 1.0  $\text{g m}^{-2}$  and subsequently stabilized (Fig. S4(b)). The filtration efficiency of PAN-10 sample ranged from 99.36% to 99.95%, with pressure drop ranging from 117.7 Pa to 265.3 Pa as the areal density was enlarged from 1.0 to 1.5  $\text{g m}^{-2}$ . The pressure drop of PAN- $x$  samples with varied fiber diameters increased linearly as the areal density of the samples increased (Fig. S4(c)), the rate at which the resistance rose might be calculated using the formula:  $y = 179x - 22.8$  on a fitted curve, where  $y$  is the pressure drop, and  $x$  is the areal density of the fibrous membrane. As the fiber diameters increased, the slope of the fitted line dropped, indicating that the fiber diameter exhibited an apparent effect on the membrane's filtration performance. As the sample's areal density grew, smaller fibers were allowed for fabrication of membranes with higher fiber packing densities and smaller average pore sizes, and more sub-micron fibers overlapped to form a thicker membrane per unit area. The internal aperture channels were vertically enlarged, which reduced the average pore sizes along the horizontal direction and improved the membrane's efficiency against sub-micron particulate matters [23]. Quality factor ( $Q_f$ ) is a critical metric for assessing the overall performance of a filter material (Fig. S4 (d)). As the areal density of fibrous membranes rose,  $Q_f$  of the material generally decreased. When the membrane's areal density exceeded 1  $\text{g m}^{-2}$ ,  $Q_f$  value of the prepared PAN-10 sample declined dramatically, indicating that the rise in areal density had a minimal effect on the overall filtration performance of the material. For PAN-14 sub-micron fibrous membrane,  $Q_f$  was relatively higher with the decrease of filtration efficiency. Therefore, to maximize the filtration performance of composite materials, it is necessary to reduce the filtration resistance as much as possible while maintaining better filtration efficiency of the fibrous membranes.

In addition, the filtration performance parameters of PAN sub-micron fiber membranes with various typologies and similar areal densities were depicted in Fig. 3(f). For PAN-10, PAN-12, and PAN-14 fibrous webs with unitary construction, filtration efficiency and pressure drop improved as the fiber diameters decreased. PAN-14 exhibited 61.3% filtration efficiency with a resistance of 29 Pa, whereas PAN-10 specimen had an excellent efficiency (99.95%) with a pressure drop of 265 Pa. However, the hierarchical-structured PAN composites with different fiber diameters for each layer displayed better filtration performance, and PAN-10/12/14 fibrous membrane revealed optimum filtration performance with  $Q_f$  of 0.04  $\text{Pa}^{-1}$ , efficiency of 99.43%, and pressure drop of 127 Pa, in which the PAN-10 fine fibrous layer mainly played an important role in improving the filtration accuracy for fine aerosol particles due to the fine fiber diameter and small pore size. Nevertheless, the coarse fibrous layers (PAN-14 and PAN-12) with larger fiber diameters extended the pore size of structural aperture channels in composite, decreasing airflow resistance (Fig. 3(c)). It was also confirmed that the hierarchical structure of the sub-micron fibrous membrane, including multiple layers with different fiber diameters and

pore sizes, had a favorable impact on enhancing the overall filtration performance.

## 3.2. Performance of the thermally bonded fibrous filters

Due to the limited mechanical strength, the electrospun fibrous webs cannot be used in practical applications without the addition of a nonwoven fabric substrate to protect them. The bonding progress for the composite materials is considerably crucial for resolving the problem of easy peeling between the two, especially in post-processing, and its impact on the composite's performance is worth being thoroughly and methodically investigated. To improve the interlaminar fracture toughness and suppress the delamination in the form of laminated nonwoven fibers in practical application, the nonwoven fabric substrates and the electrospun fibrous web were compounded via the hot-rolled and through-air bonding processes, of which the former included PB and SB processes.

### 3.2.1. Morphology and structure

The surface morphology of bonded composite materials treated by a hot-rolled process is displayed in Fig. 4(c, d), with the pristine membrane as the comparison (Fig. 4(a)). The PE/PP fibers were heated and pressed until they melted and bonded together in a block using a hot-rolled PB method (Fig. S6(b)). The core layer (electrospun fibrous web) was distorted by heating and pressing around the rolling points after the nonwoven layer was revealed, resulting in a plate-like adhesion. As displayed in Fig. 4(b, c), the produced rolling points were like the "crystalline zone" with dense structure, while the other area was similar to the "amorphous region" with fluffy spatial structure. There was a severe adhesion with large areas among fibers in the fibrous membrane (Fig. 4(d) and Fig. S6(c)), which was because the heat emitted by the roll was directly transferred to the substrate in the hot-rolled SB process. The PE/PP fibers were heated and pressed to quickly deform and bond with one another. When heat was transferred to the core layer, the electrospun membrane was deformed under pressure and even locally carbonized or adhered with PE/PP fibers, causing the fibrous membrane to be damaged and blocked in a larger area, analogue to "continuous plane"-like adhesion. To summarize, it is preferable to preserve the original microstructure and surface of the material treated using PB process rather than SB process in a hot-rolled process. Nonetheless, the former only causes structural damage to the fibrous membrane at the nip points, resulting in the formation of a local bond point, whose size is determined by the size of the engraved roll nip point.

For a through-air bonding process, fibers in the base fabric layer melted and bonded together at 130  $^{\circ}\text{C}$ , forming a compact structure that became more pronounced as treatment time increased (Fig. S6(d–f)). The melted PE/PP fibers were observed to be attached to the surface of the electrospun fibrous web (Fig. 4(f) and Fig. S6(g–i)), which corresponded to the "axon-dendrites structure" with the melted PE/PP fibers as the "axon" and the electrospun fibrous web as the "dendrites", as illustrated in Fig. 4(e). The spread of the melt fibers increased the adhesive area, which had a direct impact on the peeling strength and filtration performance of the material. Overall, the through-air temperature and time are the most important factors for the composite molding of sub-micron fibers with nonwoven fabrics.

The cross-section and surface morphology of the point-bonded and through-air composite materials are shown in Fig. 4(h–j), along with a pristine specimen for comparison. For the pristine specimen, there was an obvious delamination between the substrate fabric and the electrospun fibrous core-layer (Fig. 4(h)). Furthermore, the heat melt bonding of PE/PP fibrous surface layer with the sub-micron fibrous core layer pressed at the rolling points resulted in the relatively thinner and compacted bonding points in the point-bonded composite material (Fig. 4(i)). The material was fluffy at the non-rolling points with an intact structure, however, there was a change in material thickness in

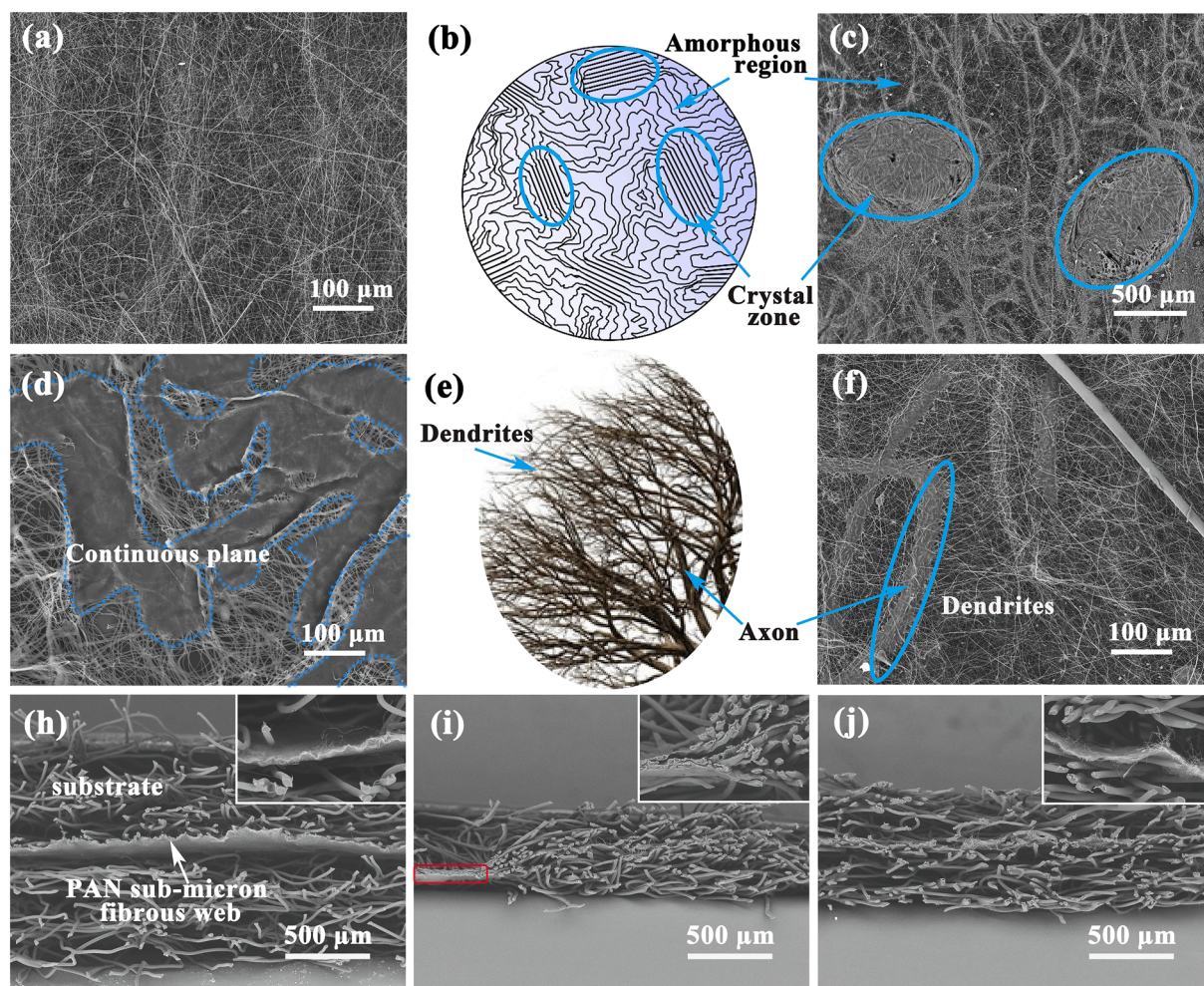


**Fig. 4.** SEM images of core-layer sub-micron fibrous webs. (a) The pristine, and (b–f) the thermal bonded materials treated via a hot-rolling process ((c) point and (d) surface bonding) and (e, f) a through-air process, and (b, e) the corresponding structural diagrams. (h–j) Cross-sectional images of (h) the pristine, (i) point-bonded, and (j) through-air composite materials.

the transition zone between the rolling point and the other area. The hot-air composite material was generally fluffy as the electrospun fibrous core-layer was not squeezed by the external extrusion (Fig. 4(j)).

### 3.2.2. Mechanical property

**3.2.2.1. Peeling strength properties.** The peeling strength test was used to assess the bonding fastness between the substrate layers and the electrospun fibrous web. The higher the stripping strength, the better the material's integration molding effect. Fig. 5(a) depicts the stripping strength of materials prepared by a hot-rolled process under different temperatures. With the same pressure (3 MPa) and feeding speed ( $1 \text{ m min}^{-1}$ ), the stripping strength of the composite material gradually increased as the treatment temperature increased. When the temperature was  $<120^\circ\text{C}$ , the composite treated by the SB process showed a negligible bonding effect among layers with stripping strength less than 1 cN, which was due to PE/PP fibers being unable to be melted with heat at temperature lower than  $120^\circ\text{C}$ . The stripping strength of the material rapidly exceeded 6 cN at a temperature of  $120^\circ\text{C}$ . The bonded material produced by PB process demonstrated a stronger bonding effect among the fibrous layers. Furthermore, as the heating temperature and pressure increased, the material's peeling strength improved, while its overall integrated structure became more prominent (Fig. 5(b)).

As shown in Fig. 5(c), the peeling strength of the through-air composite was lowest at temperature less than  $130^\circ\text{C}$  for 2 min.

Accordingly, the processing conditions are insufficient for melting PE/PP fiber skin layer components. The peeling strength of the material increased as the temperature continued to rise. The sample's peeling strength increased significantly (from 2.59 cN to 25.84 cN) as the hot-air temperature rose from  $130^\circ\text{C}$  to  $133^\circ\text{C}$ , which could be explained by the melting of PE/PP fiber cortex with the gradual increase of temperature. As a result, the bonding area between PE/PP fibers and the electrospun fibrous web gradually expanded. Similarly, with a heating temperature of  $130^\circ\text{C}$  and treatment time ranging from 2 to 4 min, the composite's peeling strength increased dramatically from 2.59 cN to 40.82 cN, indicating that the treatment time had a significant effect on the adhesion of the sample's components. However, when the heat treatment time exceeded 4 min, the increase in peeling strength slowed. This was since it took a certain amount of time to completely melt PE/PP fiber cortex, diffuse the melts, and form a bond with the electrospun fibrous webs.

**3.2.2.2. Mechanical tensile properties.** The adhesion between the primary layer and the core layer in the thermally bonded composite material has a significant impact on the mechanical properties, as well as the ease of delamination of the layers in the material with integrated structure under the effect of external force. The mechanical tensile curves of hot-rolled materials in the longitudinal and transverse directions are given in Fig. 5(d). There are two fracture peaks for both the pristine and PB- $100^\circ\text{C}$  samples (Fig. 5d(i)). The behavior could be

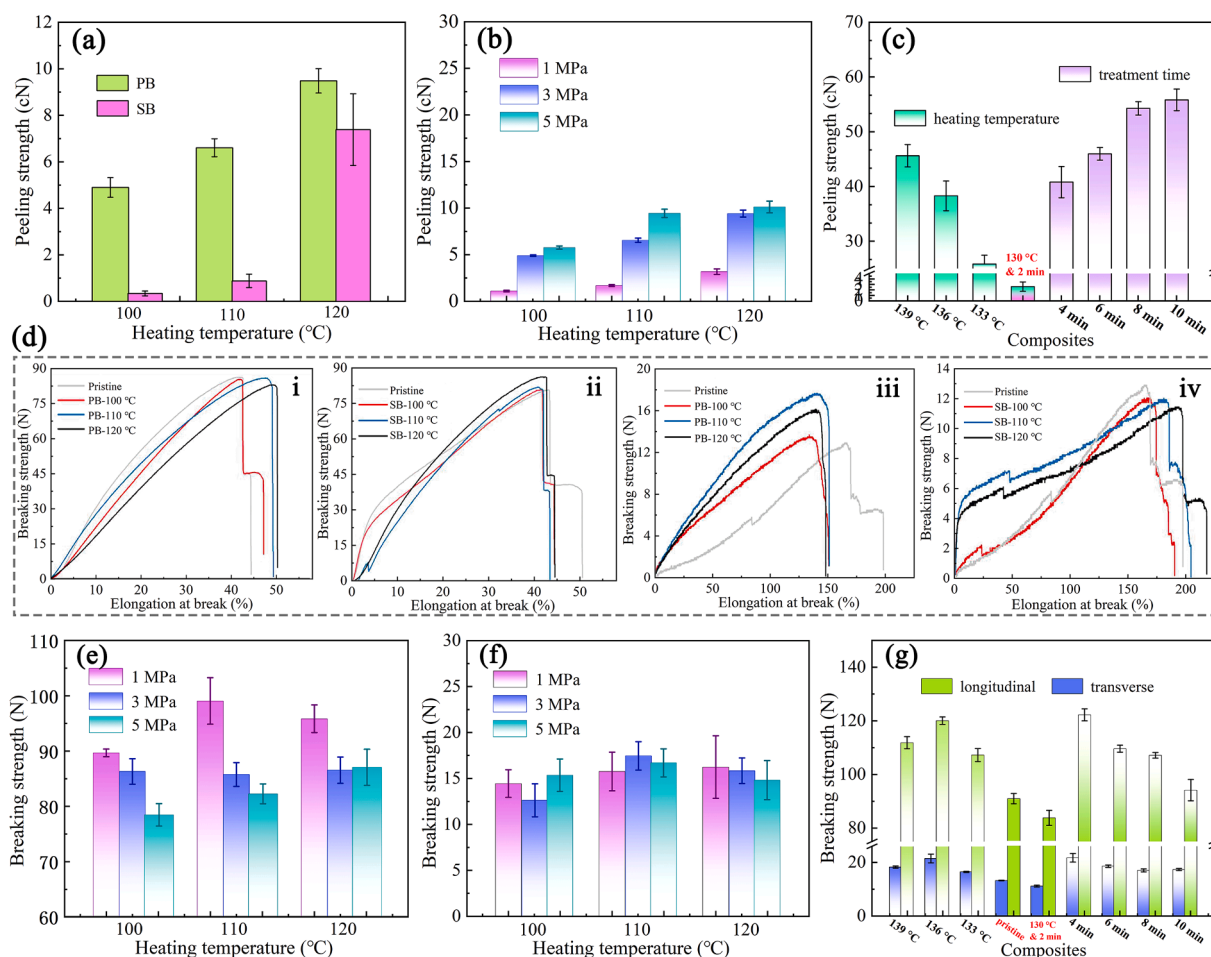


**Fig. 5.** (a–c) The stripping strength, and (d–g) breaking strength including (d (i, ii), e) the longitudinal and (d (iii, iv), f) transverse of materials prepared by (a) hot-rolled PB and SB processes under different temperatures at roll pressure of 3 MPa and speed of 1 m min<sup>-1</sup>, and (b) hot-rolled PB process with different roller temperatures and pressures, and (c, g) through-air process with different heating temperatures for 2 min and at 130 °C for various time. (d–f) The longitudinal (d (i, ii)) and transverse (d (iii, iv), f) mechanical tensile curves of the materials prepared via hot-rolled PB (d (i, iii)) and SB (d (ii, iv)) processes with different treatment temperatures (100, 110, and 120 °C) under roll pressure of 3 MPa and roll speed of 1 m min<sup>-1</sup>.

explained by the lack of adhesion between the substrate layer and the core layer. When the temperature in the hot-rolled PB process was  $\geq 110$  °C, there was only one fracture peak in the material's tensile curve, indicating that the layers in the treated material were firmly bonded together, and that there was no stripping or delamination under external force. As the treatment temperature increased, the breaking strength of the hot-rolled SB bonded material increased slightly, but the elongation at break decreased (Fig. 5d(ii)). This was related to the melting and bonding of PE/PP fibers using heat and pressure. There were two fracture peaks in the stretching curves, indicating that the inter-layer bonding forces were insufficient to resist the external forces, whereas the sample would easily peel and delaminate during the stretching process, resulting in the different fracture.

The transverse tensile curves of the materials under different hot-rolled processes are shown in Fig. 5d(iii, iv). The breaking elongation of material increased as the breaking strength decreased (Fig. 5d(iii)). Furthermore, the difference of the fracture time between layers was improved. The bonding strength between the fibrous layers was clearly sufficient to resist the external force during the stretching process, and no obvious delamination occurred with the improved synergy. The initial modulus of the materials treated in the same way but at different temperatures increased significantly (Fig. 5d(iv)). Because of the lower elasticity of the inter-layer electrospun fibrous web, there was a small breaking peak in the curve at the start of stretching. The fibrous layers gradually separated as they were stretched further. The monolayer

substrate slipped at the bonding point until it broke, and then the material was elongated and thinned until it broke. The substrate broke multiple times at various points during the process, resulting in multiple fracture peaks. In comparison, the point-bonded material possessed a better bonding effect between the layers due to the improved adhesion at the rolling points, resulting in a greater synergy in the stretching process. As a result, its breaking strength was significantly higher than that of the surface-bonded composite material.

The effect of temperature and pressure on the breaking strength of a through-air bonded composite is depicted in Fig. 5(e, f). The longitudinal and transverse breaking strength of the pristine sample were 90.76 N and 13.13 N, respectively. Comparative analysis revealed that the longitudinal breaking strength of the material decreased when the applied pressure exceeded 3 MPa, which was attributed to the damage inflicted on PE/PP fibers in the substrate layer by the increase of pressure. This was discovered to be more significant than the synergistic effect of the longitudinal stretching for the composite material. In general, the transverse fracture strength of the material increased significantly because the formed bonding points (like the "pin" structure) played a vital role in consolidating the entire structure of the composite material. These "pin" points prevented the fiber slippage during the stretching process, which increased the breaking strength.

The longitudinal and transverse breaking strengths of the samples gradually increased during the through-air process with temperature rising from 130 °C to 136 °C for 2 min (Fig. 5(g)), with the highest value

achieving at 136 °C. This was the result of a synergistic relationship between the bonding points of the electrospun fibrous web and the nonwoven fabrics. The excellent values of composite material's longitudinal and transverse breaking strengths (122.27 N and 21.87 N, respectively) were achieved at a hot-air temperature of 130 °C and a processing time of 4 min. The material's breaking strength gradually decreased as the processing time increased, an occurrence that could be attributed to the damage inflicted on the substrate material by a long heating period. It was discovered that the composite material treated at 130 °C for 2 min had a slightly lower breaking strength than the pristine material. This intriguing phenomenon was attributed to the material's fibrous layers having a relatively weaker binding effect, resulting in an easier delamination during the stretching process. Simultaneously, the single-layer substrate fabric may be damaged as a result of heating and melting. Overall, the increase of the through-air treatment temperature and time greatly improved the mechanical properties of materials.

### 3.2.3. Filtration performance

The filtration performance of the composite materials after hot-rolled bonding treatment is shown in Fig. 6(a–c). The filtration efficiencies of the composites prepared using two kinds of hot-rolled processes with the same pressure and feeding speed remained constant. With the increase of heat temperature, there was a slight fluctuation. However, the pressure drop continued to rise, and the comprehensive filtration performance of the materials deteriorated as  $Q_f$  fell. The obtained surface-bonded composite encountered higher air resistance than that of the point-bonded material at temperature above 100 °C, which was attributed to the larger adhesion areas blocking the air passage. Furthermore, when the temperature rose above the melting point of the skin-layer (-PE) component, PE/PP fibers essentially bonded, clogging the material's porous channels and reducing its filtration resistance. The pressure drops of bi-layer substrates directly treated by SB process increased linearly with heating temperature ranging from 100 °C to 120 °C (Fig. S7). This could be attributed to the substrate's

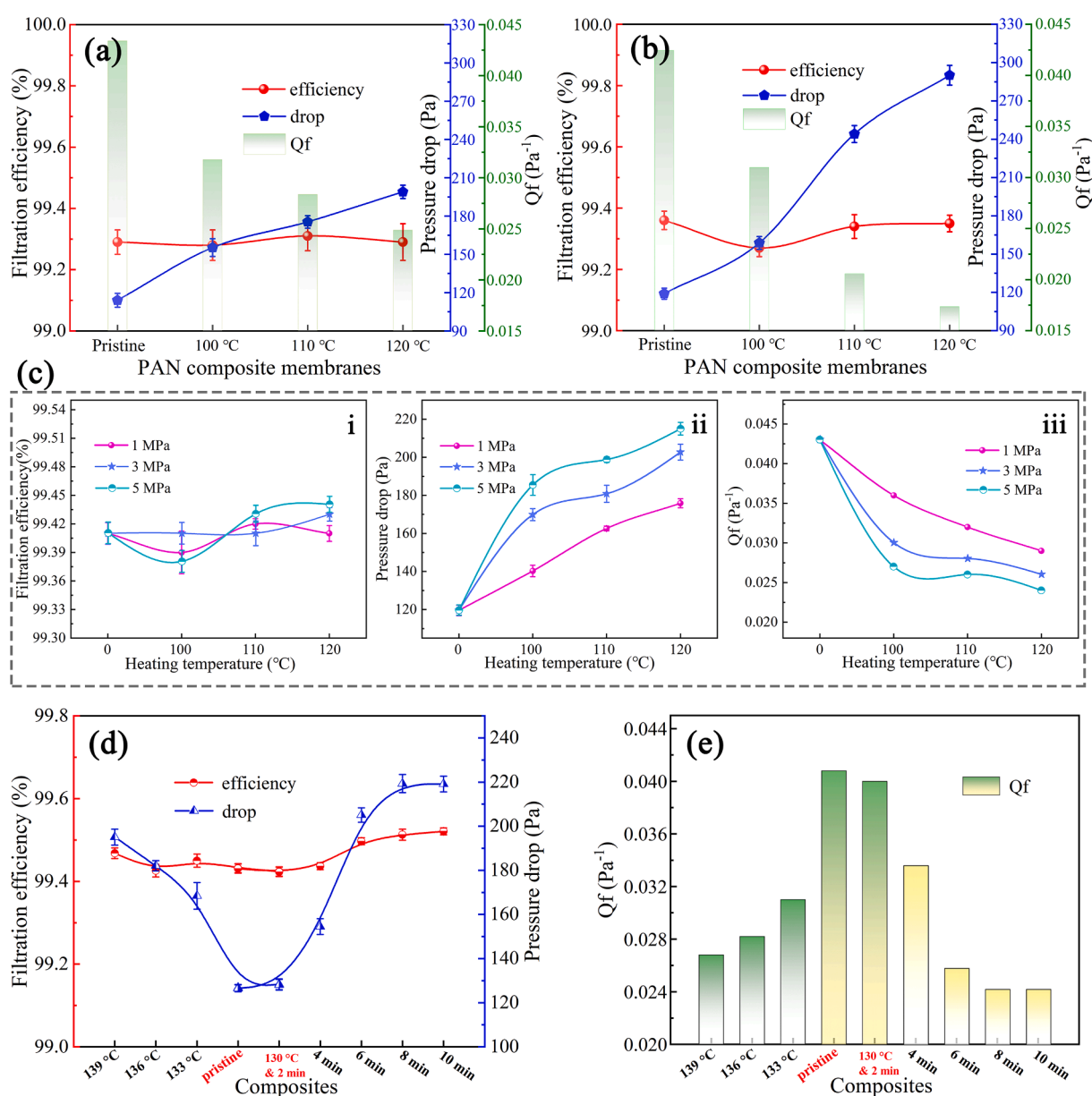


**Fig. 6.** The filtration performance of the composite materials bonded via hot-rolled (a) PB and (b) SB treatments under 3 MPa pressure and feeding speed of 1  $\text{m min}^{-1}$ , via (c) a hot-rolled PB process with different roller temperatures and pressures, and via (d, e) a through-air procedure for 2 min under different heating temperatures and treated by various time at 130 °C.

microstructure change (adhesion) and the partial blockage caused by the melting of PE/PP nonwoven fabric. The point-bonded specimen, on the other hand, had a nearly stable filtration efficiency. The increase of pressure drop for composite material was primarily where the electrospun PAN fibrous material was blocked by PE/PP fibers at the rolling points expanded as temperature increased.

In addition, the filtration performance of the composite materials treated with various parameters is interpreted in Fig. 6(c). The sample's filtration efficiency varied slightly as the heating temperature and pressing stress increased. On the other hand, there was a noticeable increase in pressure drop and a decrease in  $Q_f$  of the composites, which could be attributed to the melting and bonding together of the substrate fabric at the rolling points, which completely blocked the electrospun fibrous membrane in these locations. Furthermore, as the pressure or temperature increased, the molten components spread over a larger surface, increasing filtration resistance even further.

According to the results of the above analysis, the hot-rolled PB process had a minor impact on filtration efficiency but a significant impact on the pressure drop of the thermally bonded material. The ranges (R) of pressure drop for the three factors: temperature, pressure, and liner speed were in the order ( $R_{pre} > R_{tem} > R_{lin}$ ) in the orthogonal test results, as shown in Tables S4 and S5. As a result, the roller pressure had a greatest influence on air resistance followed by temperature, with the linear speed having the least influence. This was attributed to the small linear velocity change interval in the experimental design. The linear velocity had no effect on the pressure drop of the material at low speeds. However, an increase in roller pressure or temperature resulted in a linear increase of the material's pressure drop (Fig. S8).

The through-air treatment of the composite material allowed PE/PP fibers to adhere to electrospun fibrous webs. This, in turn, affected the material's filtration performance. For further investigation, the extent of the impact of the through-air bonding process on composite's performance is represented in Fig. 6(d, e). The filtration efficiency of the sample treated at 130 °C for 2 min was comparable to that of the pristine, while the pressure drop increased slightly. In this case, heat was insufficient to facilitate adhesion between PE/PP fibers and sub-micron fibrous webs. The filtration efficiency of the material remained unchanged as the temperature raised further, whereas the air resistance of the material increased significantly. This was attributed to the larger adhesive areas between PE/PP fibers and sub-micron fibrous webs, obstructing airflow transmission channels within the fiber membrane. Overall, the filtration performance of the materials degraded as the treatment temperature increased.

The material's filtration efficiency showed a slight upward trend as the processing time increased for the composite material treated at different time and a through-air temperature of 130 °C. When the treatment time was increased from 2 to 6 min, the sample's resistance increased significantly at first, and then slowed down, and finally stabilized due to the limited diffusivity of the molten PE/PP fiber component. When PE/PP fibers completely blocked the sub-micron fibrous webs, no new adhesion was formed, and the air resistance did not increase. As a result, the material's  $Q_f$  decreased rapidly at first, then steadily.

Based on the result of the above analysis, the sub-micron composite material treated at 130 °C for 4 min performed better than the pristine material, with a longitudinal fracture strength of 122.27 N, a transverse strength of 21.87 N, and a peeling strength of 40.82 cN. The filtration efficiency of the specimen was 99.44%, with a slightly varying pressure drop of 154.74 Pa.

### 3.2.4. Multi-index comprehensive evaluation analysis

The principal component analysis (PCA, interpreted in Supplementary information) is used to calculate the weight ( $\omega$ ) of each index in order to comprehensively evaluate the performance of materials under various process parameters. As shown in Fig. S9, the pristine sample (PB-0<sup>#</sup>) has the highest total score of 0.55, indicating that the material has an

obvious advantage in filtration performance and mechanical breaking strength. On the other hand, the composite's peeling strength is 0, which does not meet the requirements. At the same time, PB-6<sup>#</sup> and PB-5<sup>#</sup> have total scores greater than 0.5, but PB-5<sup>#</sup> exhibits superior filtration performance with the following specific comprehensive properties: 99.41% filtration efficiency, 180.67 Pa pressure drop, 6.56 cN peeling strength, 88.2 N longitudinal breaking strength, and 17.6 N transverse breaking strength. These properties match the requirements of sub-micron fibrous composite filters in practical applications very well. Furthermore, for the through-air bonded samples, the corresponding data in Table S7 after data standardization were weighted to calculate their total score under various process parameters based on the  $\omega$  of each index in Table S6. The larger the total score, the better the overall performance of the material. As shown in Fig. S7, the specimen processed at a hot-air temperature of 130 °C for 4 min showed the highest total score, implying that the overall performance of the composite material was the best. The preliminary analysis results presented above were confirmed.

### 3.3. Comprehensive comparison of thermally bonded materials prepared by hot-rolled PB and through-air bonding processes

The properties of the thermally bonded materials were further compared and investigated to exhaust differences between the two bonding processes. The composite material prepared by a through-air bonding process with 130 °C for 4 min was recorded as the through-air composite material, and the material prepared by hot-rolled PB process at 110 °C, pressure of 3 MPa, and linear speed of 1 m min<sup>-1</sup> was marked as the point-bonded composite material.

#### 3.3.1. Physical performances

**3.3.1.1. Thickness.** The thickness of the point-bonded composite material was less than that of the through-air composite, as shown in Fig. 7 (a). It was also discovered that the two bonded composites were thinner than the pristine, which corresponded to the cross-sectional morphology exhibited in Fig. 4(h-j). This phenomenon occurred as a result of PE/PP fibers melting and bonding with one another under high temperature and external force, resulting in tighter structures and smaller thickness. Furthermore, the pressure generated by the roller's force on the fibrous materials during the hot-rolled PB process was greater than the pressure generated by hot air in the through-air composite process.

**3.3.1.2. Stiffness.** The longitudinal and transverse bending stiffness of the through-air composite materials differed significantly. It was especially noticeable along the longitudinal direction, where no exact value could be measured. In the transverse direction, however, the value was lower (5.82 mN cm), indicating material possessing high flexibility (Fig. 7(b)). In contrast, the point-bonded composite material's bending stiffness in the longitudinal and transverse directions was reduced by 50% compared to the pristine sample, and its softness was greatly improved, making it suitable for the processing of pleated filter materials. Because of the faster shrinkage rate, the through-air composite material was stiffer and had a higher flexural rigidity. Fusion bonding of PE/PP fibers during post-processing increased compactness and bulk density, beneficial for direct preparation of frame or plate filter materials.

**3.3.1.3. Mechanical properties.** The through-air composite had the best tensile property, with optimal breaking strength of 21.64 MPa in the longitudinal direction and 3.87 MPa in the transverse direction, which was twice as high as that of the pristine specimen (Fig. 7(c)). However, the point-bonded composite material demonstrated a superior longitudinal breaking strength (35.48 MPa) and transverse breaking strength (7.23 MPa). Nonetheless, the peeling strength of the through-air composite material was greater than that of the point-bonded composite

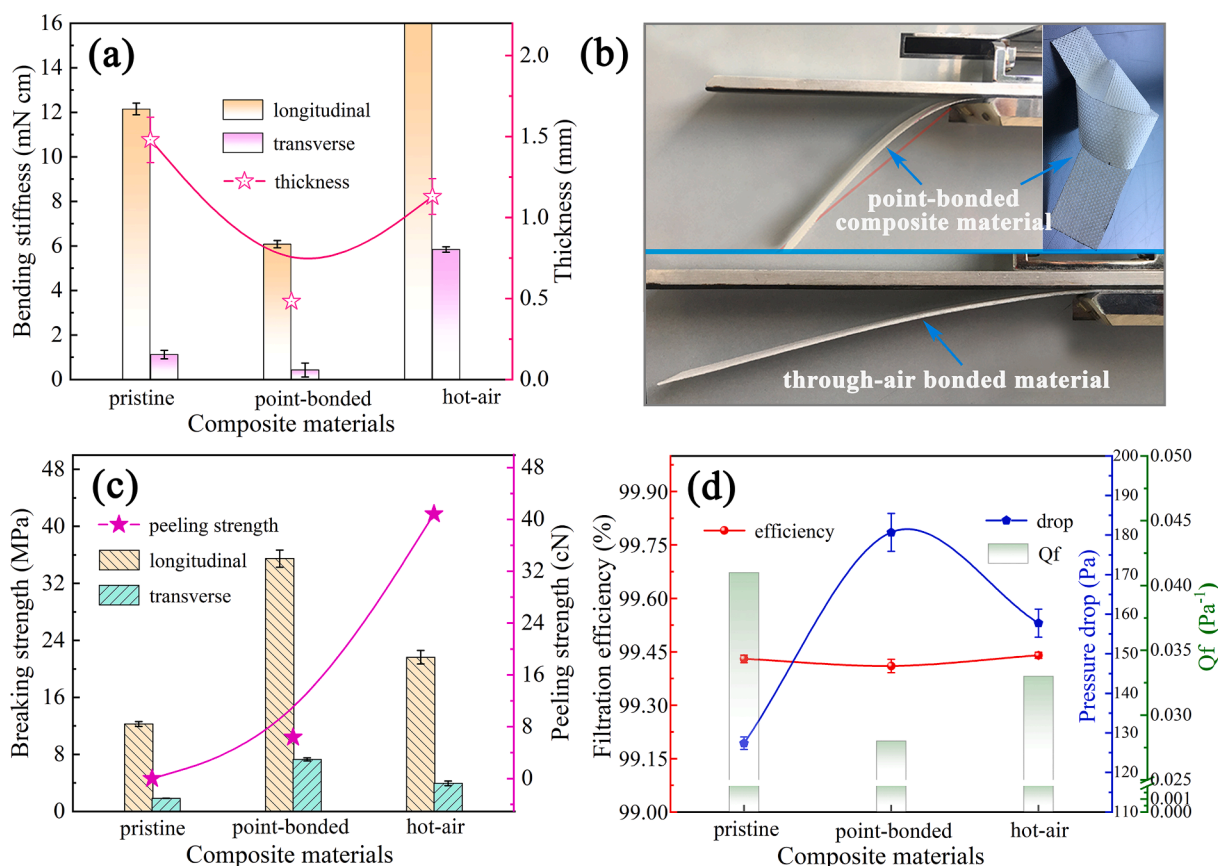


Fig. 7. (a) The distribution curves of bending stiffness and thickness, (b) photograph, (c) breaking and peeling strengths, and (d) filtration performance for the pristine, point-bonded, and through-air composite materials.

material, indicating that the integrated structure of the through-air composite material prepared was much more stable.

**3.3.1.4. Air permeability.** Air permeability is also important for the filter media, which directly reflects the performance of gas molecules passing through the fabric. As shown in Fig. S12, pristine sample possessed a better air permeability with value of  $122.3 \text{ mm s}^{-1}$ , while the permeability became poor after fibrous membrane was bonded thermally, especially through point-bonding process. The air permeability of through-air composite material grew a little worse with value of  $94.7 \text{ mm s}^{-1}$ , and the point-bonded material showed a worst permeability ( $51.6 \text{ mm s}^{-1}$ ). The results indicated that the thermally bonding process presents a negative effect on the permeability of composite materials, owing to the induced adhesion between fibers. Good permeability performance ensures the low resistance of air penetration, saving energy for filter media. Generally, the through-air fibrous composite material presented superior air permeability, which is beneficial for its practical filtration application.

### 3.3.2. Filtration performance

The filtration performance parameters of pristine, point-bonded, and through-air composite materials are shown in Fig. 7(d). There was a slight fluctuation for the filtration efficiency of three samples. In contrast, pressure drop among the three types of composite materials showed a discernible difference. Compared with the pristine, the filtration resistance of the through-air composite increased by 23.8%, significantly less than that of the point-bonded material (41.8%). The results were consistent with the air permeability of samples discussed above. The reason was that the structure was undamaged with just several adhesions between PE/PP fibers and the surface of sub-micron fibrous web for the through-air composite. While, the point-bonded

material was completely fused and bonded together at the rolling points, of which the morphology and structure were destroyed badly, possessing bad permeability, which was not beneficial for the air passing through and led to the increase of pressure drop. In general, the composite process displayed a negative impact on the filtration performance of the material. The through-air bonded composite outperformed the hot-rolled point bonded composite in terms of filtration performance while maintaining a good material integration and structural stability.

### 3.4. Filtration mechanisms of thermally bonded composite filters

The schematic diagram of the filtration mechanisms for the prepared thermally bonded composite filters is illustrated in Fig. 8. The morphology and structure of the composite materials have changed after thermally bonding, as discussed above, which affects the gas flow around the fibers and the capture of airborne particles, when compared to the pristine fibrous material (Fig. 8(a)). For the point-bonded material (Fig. 8(b)), there are two types of structures, including “crystalline zone” with dense structure and “amorphous region” with fluffy spatial structure. The airflow cannot pass through the “crystalline zone” without pores, and its streamline will turn back after hitting the “wall”, evidently increasing air resistance. Meanwhile, the airborne particles with different sizes in the gas streamline could be deposited on the surface of the “crystalline zone” primarily through sieving mechanism. The gas flow around the fibers and particle collection through composite filtration mechanisms in the other region (amorphous region) with the original morphology are the same as in the pristine sample. The surface-bonded fibrous material is scattered with “continuous planar”-like zones with no air permeability (Fig. 8(c)), where the gas flow dashes against the surface of the zones, changing the direction of the flow fluid, leading to a sharp increase of air resistance, which improves air permeability

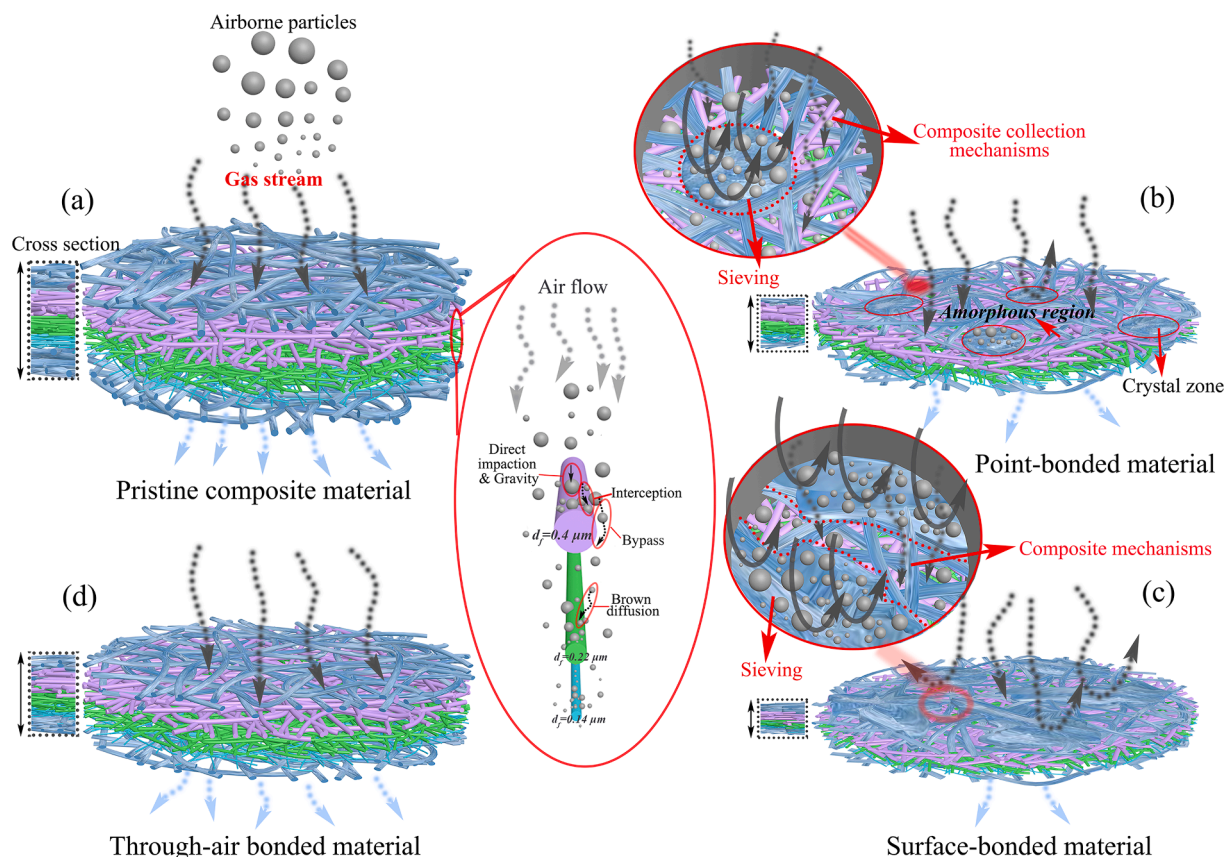


**Fig. 8.** Schematic diagrams of the filtration mechanisms for (a) the prepared pristine, (b) point-bonded, (c) surface-bonded, and (d) through-air bonded composite filters.

and increases gas velocity through rest-limited regions. Of course, the entrained particles are captured in the “continuous planar”-like zones by the sieving mechanism. In the other regions, due to the increased gas velocity, inertial impaction proves to be the more dominant means of large particle capture [24]. For the through-air bonded material with an “axon-dendrites” structure (Fig. 8(d)), the value of  $K_n$  is 0.005 for the formed “axon” region with a width of  $\sim 26 \mu\text{m}$ , so the gas flow around it belongs to the slip-flow regime where the air molecules around the fiber surface are with segmental slip flow. While the air flow around the surrounding “dendrites” with sub-micron diameter is assigned to the transition regime. It has been demonstrated that the drag force on the periphery of the “axon” is larger than that of the transition regime, due to the direct impact between air molecules and the “axon” in the slip-flow regime [25], which is the reason for the increased pressure drop of through-air bonded material.

#### 4. Conclusions

In summary, the “sandwich” structured composite fibrous membrane was fabricated using free surface electrospinning with the upper and lower protective layers made of bi-component PE/PP fibers nonwoven and the midlayer composed of the hierarchical-structured sub-micron fibrous web, which is useful for mass production of sub-micron fibrous filter media. The composite material was then thermally bonded together, allowing it to be post-processed and used in commercial productions. The effect of bonding process parameters on material’s properties was thoroughly investigated, resulting in excellent filtration and mechanical properties. The pristine composite material with a gradient-structured sub-micron fibrous web as the midlayer and an areal density of  $1.5 \text{ g m}^{-2}$  demonstrated superior filtration performance with filtration efficiency of 99.43% and pressure drop of 127.4 Pa for aerosol

particles with a diameter of 260 nm under airflow velocity of  $5.33 \text{ cm s}^{-1}$ . A through-air bonded composite material with favorable morphology and structure exhibited greater rigidity, and better physical properties (peeling strength, mechanical breaking strength) and filtration performance than that of a hot-rolled bonded material. The composite material possessed the best formability, superior peeling strength, and breaking strength after through-air bonding treatment at  $130 \text{ }^\circ\text{C}$  for 4 min, with filtration efficiency of 99.44% and a slightly increased pressure drop. The property-enhanced composite material, composed of hierarchical-structured sub-micron fibrous webs and nonwoven fabrics using a save-energy and low-cost through-air thermally bonding process with high yield fabrication, demonstrated promising commercial and industrial productions.

#### CRediT authorship contribution statement

**Mengjuan Zhou:** Formal analysis, Data curation, Writing – original draft. **Lulu Shi:** Investigation, Writing – original draft. **Hongyu Dai:** Conceptualization, Validation, Data curation. **Akampunguza Obed:** Validation, Writing – review & editing. **Penghong Liu:** Methodology, Writing – review & editing. **Jiajun Wu:** Resources, Software. **Xiaohong Qin:** Supervision, Funding acquisition. **Rongwu Wang:** Visualization, Project administration.

#### Declaration of Competing Interest

The authors declare that they have no known competing financial interests or personal relationships that could have appeared to influence the work reported in this paper.

## Acknowledgments

This work was partly supported by the Fundamental Research Funds for the Central Universities (2232020D-15, 2232020A-08, 2232020G-01, 2232020D-14 and 2232019D3-11) and grants (51773037, 51973027, 51803023, 52003044 and 61771123) from the National Natural Science Foundation of China. This work has also been supported by the Chang Jiang Scholars Program and the Innovation Program of Shanghai Municipal Education Commission (2019-01-07-00-03-E00023) to Prof. Xiaohong Qin, and the Fundamental Research Funds for the Central Universities and Graduate Student Innovation Fund of Donghua University (CUSF-DH-D-2019051) to Ms. Mengjuan Zhou.

## Appendix A. Supplementary material

Supplementary data to this article can be found online at <https://doi.org/10.1016/j.seppur.2022.120726>.

## References

- [1] B. Brunekreef, Air pollution and human health: from local to global issues, *Procedia Soc. Behav. Sci.* 2 (2010) 6661–6669, <https://doi.org/10.1016/j.sbspro.2010.05.010.1>.
- [2] K. Donaldson, V. Stone, A. Seaton, W. MacNee, Ambient particle inhalation and the cardiovascular system: potential mechanisms, *Environ. Health Persp.* 109 (2001) 523–527, <https://doi.org/10.2307/3454663>.
- [3] T.D. Nelin, A.M. Joseph, M.W. Gorr, L.E. Wold, Direct and indirect effects of particulate matter on the cardiovascular system, *Toxicol. Lett.* 208 (3) (2012) 293–299, <https://doi.org/10.1016/j.toxlet.2011.11.008>.
- [4] S. Feng, C. Shen, N. Xia, W. Song, M. Fan, B.J. Cowling, Rational use of face masks in the COVID-19 pandemic, *Lancet Respir. Med.* 8 (5) (2020) 434–436, [https://doi.org/10.1016/S2213-2600\(20\)30134-X](https://doi.org/10.1016/S2213-2600(20)30134-X).
- [5] Y. Bai, L. Yao, T. Wei, F. Tian, D.-Y. Jin, L. Chen, M. Wang, Presumed asymptomatic carrier transmission of COVID-19, *Jama* 323 (2020) 1406–1407, <https://doi.org/10.1001/jama.2020.2565>.
- [6] Z. Zhang, D. Ji, H. He, S. Ramakrishna, Electrospun ultrafine fibers for advanced face masks, *Mater. Sci. Eng. R* 143 (2021) 100594, <https://doi.org/10.1016/j.mser.2020.100594>.
- [7] P. Li, C. Wang, Y. Zhang, F. Wei, Air filtration in the free molecular flow Regime: A review of high-efficiency particulate air filters based on carbon nanotubes, *Small* 10 (22) (2014) 4543–4561, <https://doi.org/10.1002/sml.201401553>.
- [8] C.-S. Wang, Y. Otani, Removal of nanoparticles from gas streams by fibrous filters: A review, *Ind. Eng. Chem. Res.* 52 (1) (2013) 5–17, <https://doi.org/10.1021/ie300574m>.
- [9] J.H. Vincent, *Air filtration: an integrated approach to the theory and applications of fibrous filters*, Pergamon Press, Oxford, England, 1995 [https://doi.org/10.1016/0021-8502\(95\)90072-1](https://doi.org/10.1016/0021-8502(95)90072-1).
- [10] C.N. Davies, *Air filtration*, Academic Press, London, 1973.
- [11] K. Jayaraman, M. Kotaki, Y. Zhang, X. Mo, S. Ramakrishna, Recent advances in polymer nanofibers, *J. Nanosci. Nanotechnol.* 4 (2004) 52–65, <https://doi.org/10.1166/jnn.2004.078>.
- [12] R. Barhate, S. Ramakrishna, Nanofibrous filtering media: Filtration problems and solutions from tiny materials, *J. Membr. Sci.* 296 (1-2) (2007) 1–8, <https://doi.org/10.1016/j.memsci.2007.03.038>.
- [13] W.-F. Leung, C.-H. Hung, P.-T. Yuen, Effect of face velocity, nanofiber packing density and thickness on filtration performance of filters with nanofibers coated on a substrate, *Sep. Purif. Technol.* 71 (1) (2010) 30–37, <https://doi.org/10.1016/j.seppur.2009.10.017>.
- [14] Z. Wang, Z. Pan, Preparation of hierarchical structured nano-sized/porous poly (lactic acid) composite fibrous membranes for air filtration, *Appl. Surf. Sci.* 356 (2015) 1168–1179, <https://doi.org/10.1016/j.apsusc.2015.08.211>.
- [15] J. Xiong, M. Zhou, H. Zhang, Z. Quan, X. Qin, R. Wang, Sandwich-structured fibrous membranes with low filtration resistance for effective PM2.5 capture via one-step needless electrospinning, *Mater. Res. Express* 6 (2019) 1–8, <https://doi.org/10.1088/2053-1591/aaf760>.
- [16] C. Chu, Development of extra-sonic composite geotextile, 20 (2002) 14–17.
- [17] X.Y. Wang, R.H. Gong, Thermal oxidative degradation of bicomponent PP/PET fiber during thermal bonding process, *J. Appl. Polym. Sci.* 104 (1) (2007) 391–397, <https://doi.org/10.1002/app.24875>.
- [18] R.H. Gong, C. Fang, I. Porat, Thermal bonding of 3D nonwoven shells, *Int. Nonwoven J.* 9 (2000) 20.
- [19] R.H. Gong, C. Fang, I. Porat, Single process production of 3D nonwoven shell structures: Part 2 CFD modelling of thermal bonding process, *Int. Nonwoven J.* 10 (2001) 24, <https://doi.org/10.1177/15589250010s1000108>.
- [20] N. Vinh, H.-M. Kim, Electrospinning Fabrication and Performance Evaluation of Polyacrylonitrile Nanofiber for Air Filter Applications, *Appl. Sci.* 6 (9) (2016) 235, <https://doi.org/10.3390/app6090235>.
- [21] M. Zhou, M. Fang, Z. Quan, H. Zhang, X. Qin, R. Wang, J. Yu, Large-scale preparation of micro-gradient structured sub-micro fibrous membrane with narrow diameter distribution for high-efficiency air purification, *Environ. Sci. Nano* 12 (2019) 3560–3578, <https://doi.org/10.1039/c9en00816k>.
- [22] Y. Liu, M. Park, B. Ding, J. Kim, M. El-Newehy, S.S. Al-Deyab, H.-Y. Kim, Facile electrospun Polyacrylonitrile/poly(acrylic acid) nanofibrous membranes for high efficiency particulate air filtration, *Fibers Polym.* 16 (3) (2015) 629–633, <https://doi.org/10.1007/s12221-015-0629-1>.
- [23] M. Zhou, M. Hu, Z. Quan, H. Zhang, X. Qin, R. Wang, J. Yu, Polyacrylonitrile/polyimide composite sub-micro fibrous membranes for precise filtration of PM<sub>0.26</sub> pollutants, *J. Colloid Interf. Sci.* 578 (2020) 195–206, <https://doi.org/10.1016/j.jcis.2020.05.081>.
- [24] C. Yang, Aerosol filtration application using fibrous media-an industrial perspective, *Chinese J. Chem. Eng.* 20 (2012) 1–9.
- [25] X. Zhao, S. Wang, X. Yin, J. Yu, B. Ding, Slip-effect functional air filter for efficient purification of PM<sub>2.5</sub>, *Sci. Rep.* 6 (2016) 35472, <https://doi.org/10.1038/srep35472>.